

## Enhancing The Mode Conversion Efficiency In JET Plasmas With Multiple Mode Conversion Layers

D. Van Eester, E. Lerche, T. Johnson, T. Hellsten, J. Ongena et al.

Citation: *AIP Conf. Proc.* **1406**, 301 (2011); doi: 10.1063/1.3664981

View online: <http://dx.doi.org/10.1063/1.3664981>

View Table of Contents: <http://proceedings.aip.org/dbt/dbt.jsp?KEY=APCPCS&Volume=1406&Issue=1>

Published by the [American Institute of Physics](#).

---

### Related Articles

Phase space structure of the electron diffusion region in reconnection with weak guide fields

[Phys. Plasmas 19, 112108 \(2012\)](#)

Average atom transport properties for pure and mixed species in the hot and warm dense matter regimes

[Phys. Plasmas 19, 102709 \(2012\)](#)

Hot-electron generation by “cavitating” Langmuir turbulence in the nonlinear stage of the two-plasmon–decay instability

[Phys. Plasmas 19, 102708 \(2012\)](#)

Spherical torus equilibria reconstructed by a two-fluid, low-collisionality model

[Phys. Plasmas 19, 102512 \(2012\)](#)

Space-charge-based electrostatic plasma confinement involving relaxed plasma species

[Phys. Plasmas 19, 102510 \(2012\)](#)

---

### Additional information on AIP Conf. Proc.

Journal Homepage: <http://proceedings.aip.org/>

Journal Information: [http://proceedings.aip.org/about/about\\_the\\_proceedings](http://proceedings.aip.org/about/about_the_proceedings)

Top downloads: [http://proceedings.aip.org/dbt/most\\_downloaded.jsp?KEY=APCPCS](http://proceedings.aip.org/dbt/most_downloaded.jsp?KEY=APCPCS)

Information for Authors: [http://proceedings.aip.org/authors/information\\_for\\_authors](http://proceedings.aip.org/authors/information_for_authors)

### ADVERTISEMENT



AIP Advances

*Submit Now*

Explore AIP's new  
open-access journal

- Article-level metrics now available
- Join the conversation! Rate & comment on articles

# Enhancing The Mode Conversion Efficiency In JET Plasmas With Multiple Mode Conversion Layers

D. Van Eester<sup>a</sup>, E. Lerche<sup>a</sup>, T. Johnson<sup>b</sup>, T. Hellsten<sup>b</sup>, J. Ongena<sup>a</sup>, M.-L. Mayoral<sup>c</sup>, D. Frigione<sup>d</sup>, C. Sozzi<sup>e</sup>, G. Calabro<sup>d</sup>, M. Lennholm<sup>f</sup>, P. Beaumont<sup>c</sup>, T. Blackman<sup>c</sup>, D. Brennan<sup>c</sup>, A. Brett<sup>c</sup>, M. Cecconello<sup>g</sup>, I. Coffey<sup>c</sup>, A. Coyne<sup>c</sup>, K. Crombe<sup>h</sup>, A. Czarnecka<sup>9</sup>, R. Felton<sup>c</sup>, M. Gatu Johnson<sup>f</sup>, C. Giroud<sup>c</sup>, G. Gorini<sup>e</sup>, C. Hellesen<sup>g</sup>, P. Jaquet<sup>c</sup>, Y. Kazakov<sup>j</sup>, V. Kiptily<sup>c</sup>, S. Knipe<sup>c</sup>, A. Krasilnikov<sup>k</sup>, Y. Lin<sup>l</sup>, M. Maslov<sup>m</sup>, I. Monakhov<sup>c</sup>, C. Noble<sup>c</sup>, M. Nocente<sup>c</sup>, L. Pangioni<sup>c</sup>, I. Proverbio<sup>e</sup>, M. Stamp<sup>c</sup>, W. Studholme<sup>c</sup>, M. Tardocchi<sup>e</sup>, T.W. Versloot<sup>n</sup>, V. Vdovin<sup>o</sup>, A. Whitehurst<sup>c</sup>, E. Wooldridge<sup>c</sup>, V. Zoita<sup>p</sup> and JET EFDA Contributors\*

*JET-EFDA Culham Science Centre, Abingdon, OX14 3DB, UK*

<sup>a</sup>LPP-ERM/KMS, Association Euratom-‘Belgian State’, TEC Partner, Brussels, Belgium, <sup>b</sup>Fusion Plasma Physics, Association Euratom-VR, KTH, Stockholm, Sweden, <sup>c</sup>Euratom-CCFE Fusion Association, Culham Science Centre, UK, <sup>d</sup>Euratom-ENEA sulla Fusione, C. R. Frascati, Frascati, Italy, <sup>e</sup>Instituto di Fisica del Plasma, EURATOM-ENEA-CNR Association, Milan, Italy, <sup>f</sup>EFDA Close Support Unit, Culham Science Centre, Abingdon OX14 3DB, UK & European Commission, B-1049 Brussels, Belgium, <sup>g</sup>Uppsala University, Association EURATOM-VR, <sup>h</sup>Department of Applied Physics, Ghent University, B-9000 Ghent, Belgium, <sup>i</sup>Institute of Plasma Physics and Laser Microfusion, Warsaw, Poland, Uppsala, Sweden, <sup>j</sup>V.N. Karazin Kharkiv National University, Kharkiv, Ukraine, <sup>k</sup>SRF RF Troitsk Institute for Innovating and Fusion Research, Troitsk, Russia, <sup>l</sup>MIT Plasma Science and Fusion Center, Cambridge, MA 02139, USA, <sup>m</sup>CRPP-EPFL, Association Euratom-Confédération Suisse, CH-1015 Lausanne, Switzerland, <sup>n</sup>FOM Institute Rijnhuizen, Association EURATOM-FOM, Nieuwegein, the Netherlands, <sup>o</sup>RNC Kurchatov Institute, Nuclear Fusion Institute, Moscow, Russia, <sup>p</sup>Association EURATOM-MEdC, National Institute for Plasma Physics, Bucharest, Romania

**Abstract.** The constructive interference effect described by Fuchs et al. [1] shows that the mode conversion and thereby the overall heating efficiency can be enhanced significantly when an integer number of fast wave wavelengths can be folded in between the high field side fast wave cutoff and the ion-ion hybrid layer(s) at which the ion Bernstein or ion cyclotron waves are excited. This effect was already experimentally identified in (<sup>3</sup>He)-D plasmas [2] and was recently tested in (<sup>3</sup>He)-H JET plasmas. The latter is an ‘inverted’ scenario, which differs significantly from the (<sup>3</sup>He)-D scenarios since the mode-conversion layer is positioned between the low field side edge of the plasma and the ion-cyclotron layer of the minority <sup>3</sup>He ions (whereas the order in which a wave entering the plasma from the low field side encounters these layers is inverted in a ‘regular’ scenario), and because much lower <sup>3</sup>He concentrations are needed to achieve the mode-conversion heating regime. The presence of small amounts of <sup>4</sup>He and D in the discharges gave rise to an additional mode conversion layer on top of the expected one associated with <sup>3</sup>He-H, which made the interpretation of the results more complex but also more interesting: Three different regimes could be distinguished as a function of  $X[{}^3\text{He}]$ , and the differing dynamics at the various concentrations could be traced back to the presence of these

---

\* See the Appendix of F. Romanelli et al., Proceedings of the 23rd IAEA Fusion Energy Conference 2010, Daejeon, Korea

two mode conversion layers and their associated fast wave cutoffs. Whereas (1-D and 2-D) numerical modeling yields quantitative information on the RF absorptivity, recent analytical work by Kazakov [3] permits to grasp the dominant underlying wave interaction physics.

**Keywords:** ICRF heating, mode conversion, constructive/destructive interference

**PACS:** 52.35.Hr, 52.50.Qt, 52.65.Ff

## INTRODUCTION

Mode conversion heating has become one of the standard tools to do transport analysis and is often used in rotation experiments (see e.g. [3-5]). It relies on the excitation by the fast wave (FW) launched by standard ICRF antennas of short wavelength modes at the ion-ion hybrid (IIH) resonance. The latter modes are efficiently damped on electrons in a narrow region of the plasma. The interference effect described by Fuchs et al. [1] allows to significantly enhance the mode conversion and thereby the overall RF heating efficiency when the machine and plasma parameters are chosen such that an integer number of FW wavelengths can be folded in between the high field side (HFS) FW cutoff and the IIH layer. This effect was already experimentally identified in ( $^3\text{He}$ )-D plasmas [2] and was recently tested in ( $^3\text{He}$ )-H JET plasmas.

Before going to its activated phase, ITER would be run at 2.65T i.e. half its nominal magnetic field and using Hydrogen plasmas. From the ICRF (ion cyclotron resonance frequency) heating point of view, ( $^3\text{He}$ )-H plasmas at 2.65T are an exact mock-up of the D-T plasmas at full-field: The  $Z/A$  values of H and  $^3\text{He}$  ions ( $Z$ : charge number,  $A$ : mass number) differ by a factor of 2 with those of D and T and hence the relative positions of the cyclotron layers are identical when running at half the field. Recent JET experiments examined the potential of the fundamental ( $N=1$ , where  $N$  is the cyclotron harmonic number) H majority heating and the second harmonic ( $N=2$ )  $^3\text{He}$  heating at ITER's half field [6,7]. By merely changing the magnetic field to 3.4T, minority and mode conversion wave heating in ( $^3\text{He}$ )-H was also studied. Mayoral et al. examined the ICRF heating of such plasmas at very low  $^3\text{He}$  concentrations ( $X[^3\text{He}] < 3\%$ ) [8] and found that the mode conversion regime was already reached at  $X[^3\text{He}] \sim 2-3\%$ , in contrast to the  $\sim 10-15\%$  needed to make the mode conversion efficient in regular scenarios. These experiments also brought to light the sensitivity of inverted scenarios to the plasma composition: the small quantities of Carbon unavoidably present in JET plasmas (up to 2010, the JET inner vessel was covered with C tiles) shifted the mode conversion layer over a distance of  $\sim 0.2\text{m}$  away from where it was expected to lie in a pure  $^3\text{He}$ -D plasma.

The more recent ( $^3\text{He}$ )-H experiments focused on studying the higher  $X[^3\text{He}]$  range and in particular addressed the questions "How can the mode conversion efficiency be optimized?" and "Can significant plasma flow be generated in the mode conversion regime?" The present paper addresses the first question.

## EXPERIMENTAL RESULTS

During the recent mode conversion studies in JET in ( $^3\text{He}$ )-H plasmas two types of discharges were used. One type of discharges was intended to shed light on the Fuchs effect while the focus in the others was the analysis of RF induced plasma rotation. In the former, the ICRF power was modulated throughout the flat-top of the discharge

and a modulation frequency of 4Hz was used. In the latter, beam blips with a duration of 100ms were used to assess the toroidal and poloidal bulk plasma rotation. As the fast beam particles tend to drag along and speed up the plasma via Coulomb collisions, the time intervals during which the diagnostic beam is fired are short compared to the flat top time. In between beam blips RF power modulation at 25Hz was applied. No H beam was available and thus a D beam was used. Hence it is necessary to assess how the ICRF power affects this D population.

The applied RF power level was typically  $\sim 4\text{MW}$ , brought back to half that value during slow modulation and to only 15% of the maximal value during fast modulation. The 4Hz slow modulation allows studying the response both of the ion and of the electron temperature to the RF power change. The electron temperature is obtained from electron cyclotron emission (ECE), while the ion temperature is obtained from charge exchange measurements. Also global signals (such as the diamagnetic energy or the plasma energy) can be studied. The charge exchange diagnostic beam is left on during the whole discharge in the first type of shots, while it is only on during the NBI blips in the second type of shots. The 25Hz modulation is too fast to capture the ion dynamics and solely allows studying the electron response. In spite of this drawback, the fast modulation is extremely useful as it is not suffering from the effects of heat wave diffusion away from the heat source and thus allows a better understanding of what the actual electron power deposition profile looks like.

The applied frequency is  $\sim 32\text{MHz}$  and the toroidal magnetic field on the geometric axis ( $R_0=2.97\text{m}$ ) is  $B_0=3.41\text{T}$ . Dipole ( $0 \pi 0 \pi$ ) phasing is used in low triangularity plasmas such that the last closed flux surface is as parallel as possible to the A2 antennae to optimize coupling. The modest auxiliary power input leaves the plasma in L-mode. For the chosen parameters the  $N=1$   $^3\text{He}$  cyclotron layer lies slightly ( $\sim 0.24\text{m}$ ) on the low field side of the plasma core while the  $N=1$  H cyclotron layer is outside the machine on the low field side. The cold  $N=1$  D layer lies on the high field side but ICRF heated D beam particles will absorb wave power at their Doppler shifted resonance layer, which is closer to the plasma core.

Figure 1 shows the time evolution of several key variables of two discharges at different  $^3\text{He}$  concentrations.  $X[^3\text{He}]$  is controlled via a real time control scheme relating relative light intensity to relative concentrations steering the  $^3\text{He}$  gas injection valve (see [2] and the references therein). The  $^3\text{He}$  concentration is scanned from 1 to 4% in discharge #79343 and from 3% to 12% in shot #79352 (Fig. 1d). In both discharges the response of the radiated power (Fig. 1b), the electron temperature (Fig. 1g) and the MHD energy (Fig. 1f) to the modulation of the ICRF power (Fig. 1a) is clearly visible while the electron density response is weaker and the response of the ion temperature (Fig. 1h) is absent. Note that the RF system struggles to couple power at the start of discharge #79352 and the end of discharge #79343, when the  $^3\text{He}$  concentration is about 5% in both shots. Also the electron temperature response to the RF modulation is correlated with the  $^3\text{He}$  concentration in the same way, showing the typical periodic increase and decrease as a result of the two alternatingly applied power levels. For the imposed ICRF power of 3-4MW, core temperatures of 3-4keV are reached by the electrons, and slightly less (2-3keV) by the ions. Except for the radiated power, all signals for shot #79352 increase for increasing  $^3\text{He}$  concentration.

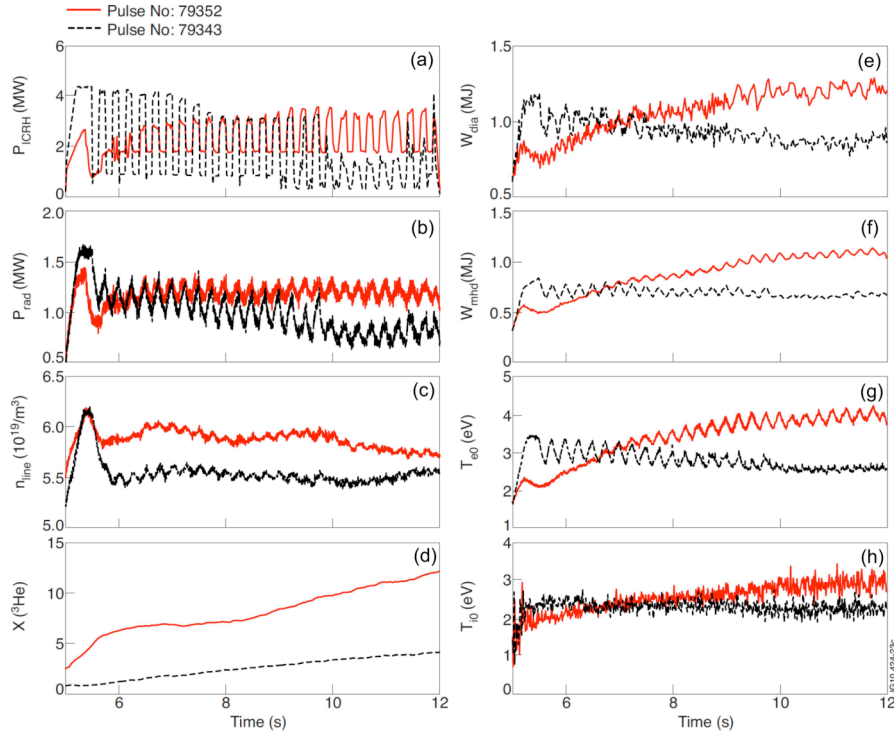


**FIGURE 1.** Overview of some characteristic quantities for shots 79343 (with a modest  $X[{}^3\text{He}]$  scan) and 79352 (in which  $2.5\% < X[{}^3\text{He}] < 12\%$ ): (a) modulated ICRH power, (b) radiated power, (c) line integrated density for a chord through the plasma center, (d) real time control estimate of the  ${}^3\text{He}$  concentration, (e) diamagnetic energy, (f) plasma energy, (g) central electron temperature and (h) central ion temperature.

Figure 2 depicts the diamagnetic energy (Fig. 2a), the neutron rate (Fig. 2b), the core electron temperature (Fig. 2c) and the antenna strap resistance (Fig. 2d) as a function of the  ${}^3\text{He}$  minority concentration for a number of data points at similar densities of  $5.5 - 6 \times 10^{19}/\text{m}^3$ . The diamagnetic energy, the electron temperature and the antenna resistance all exhibit a maximum at low  ${}^3\text{He}$  concentrations, and fall sharply when reaching the first mode conversion regime. Between  $X[{}^3\text{He}] = 3-5\%$ , the overall performance is poor. It recovers and becomes even better than at low concentrations in the second mode conversion regime ( $X[{}^3\text{He}] > 6\%$ ). It is worthwhile to note that the minority heating regime at low concentrations is not accompanied by a noticeable neutron yield, but that this quantity rises pronouncedly in the second mode conversion regime (Fig. 2b), suggesting that fast D ions are created. This is confirmed experimentally by  $\gamma$ -ray measurements: NBI D ions needed to have ion temperature data from the charge exchange diagnostic are non-intentionally accelerated by the RF waves at their Doppler shifted resonance (for more details, see [2,9]).

The sharp drop on the heating efficiency observed in the intermediate  $X[{}^3\text{He}]$  region is not solely a consequence of the wave dynamics near the ion-ion hybrid layer but is also related to poor RF power coupling associated to a FW cut-off located at the LFS of the plasma. In Fig. 2d it can be seen that in the  ${}^3\text{He}$  concentration intervals in which good heating efficiency is observed the antenna resistance is high, and that it falls away when approaching  $X[{}^3\text{He}]$  of 3-6% from either side. This correlation with the concentration can directly be observed on the coupled RF power level and on the

resistance of individual straps, respectively higher and more responding to the modulation at low  $X[{}^3\text{He}] \sim 1\text{-}2\%$  than at intermediate concentrations of  $2\text{-}4\%$ .

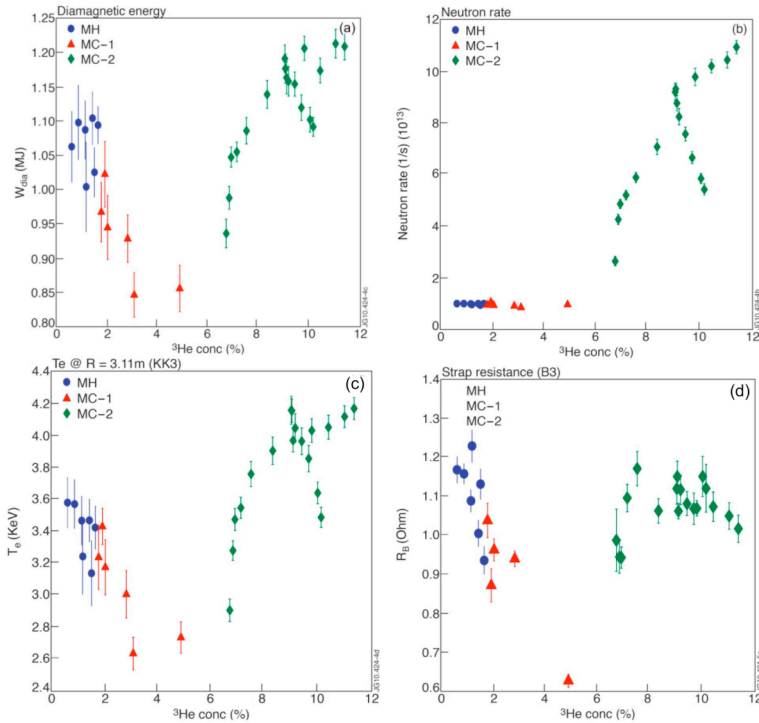


**FIGURE 2.** Dependence of (a) the diamagnetic energy, (b) the neutron rate, (c) the electron temperature and (d) the B3 antenna strap resistance on  $X[{}^3\text{He}]$ .

That the  ${}^3\text{He}$  concentration is a key parameter in the examined shots is clearly seen in Fig. 3. Both at low (Fig. 3a) and at high (Fig. 3b) concentration the maximum absorbed power density (mode conversion loci) shifts outward for increasing  ${}^3\text{He}$  concentration. At low concentration the maximum moves out rapidly for increasing  $X[{}^3\text{He}]$  (the minor radius position shifting from  $\rho_{\text{max}} \sim 0.4\text{m}$  when  $X[{}^3\text{He}] = 2.5\%$  to  $\rho_{\text{max}} \sim 0.55\text{m}$  when  $X[{}^3\text{He}] = 3.3\%$ ). At higher concentrations the position of the power density maximum seems to be less affected by the  ${}^3\text{He}$  content of the plasma. At first sight the location of the maxima seems puzzling: the fast-moving maximum seems to disappear at higher concentrations, and a new maximum enters the picture close to the plasma centre. This seeming inconsistency is a result of the dependence of the mode conversion layer position on the composition of the plasma (see further).

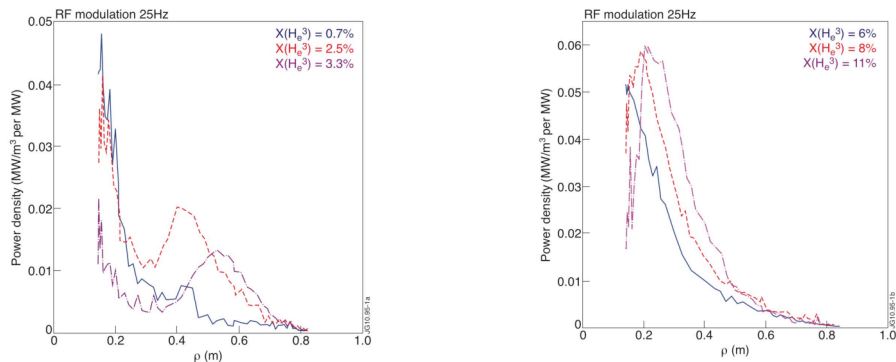


**FIGURE 3.** Electron RF power deposition profiles for various  $X[{}^3\text{He}]$ .

The results of the RF absorption efficiency analysis as a function of the  $^3\text{He}$  concentration are summarized in Fig. 4. The full dots represent the absorption by the ions, electrons and the summed power obtained from analyzing the charge exchange and ECE temperature profiles. The total heating efficiency obtained by performing a Fourier analysis on the global MHD energy is depicted as diamonds. The two are in reasonable agreement, although the heating efficiency derived from the MHD energy tends to be somewhat higher than the heating efficiency derived using the RF power absorption profiles. Taking into account that e.g. the ion temperature signal is somewhat noisy, one possible explanation is that this difference is due to the intrinsic inaccuracy of the diagnostics. The difference may, more likely, simply be due to the fact that some physics aspects are not (well) captured by some of the diagnostics: e.g. both the reconstituted electron and ion temperature tend to be asymmetric w.r.t. to the magnetic axis, suggesting that effects such as trapping of non-thermalized populations should be taken into account. Particularly at lower concentrations ( $X[^3\text{He}] \sim 1\%$ ), part of the RF power is expected to be absorbed by the  $^3\text{He}$  ions and the (bulk) temperatures do not account for the energy carried by fast subpopulations.

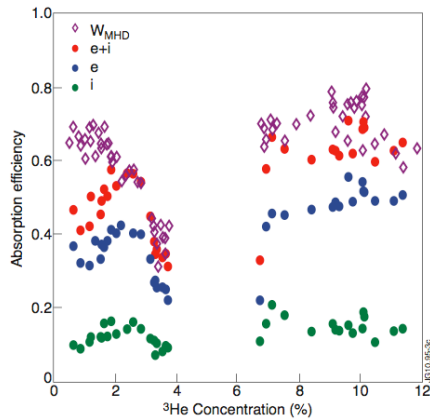


**FIGURE 4.** Heating efficiency as a function of  $X[^3\text{He}]$ .

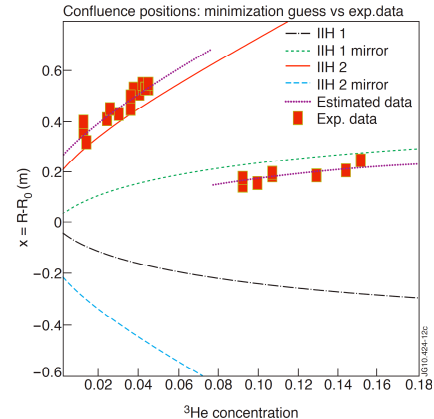


**FIGURE 5.** Result of the minimization procedure to infer the plasma composition based on the confluence layer positions as function of  $X[^3\text{He}]$ .

Figure 4 confirms the several distinct heating regimes observed as a function  $X[^3\text{He}]$ . At low  $^3\text{He}$  concentration the “bulk” heating efficiency grows with  $X[^3\text{He}]$  up to  $X[^3\text{He}] \sim 2-2.5\%$ . In this region the MHD energy results (diamonds) indicate a higher heating efficiency than the results derived from the T-profile analysis. Beyond the maximum at  $X[^3\text{He}] \sim 2\%$ , the heating efficiency degrades quickly. In this region the MHD energy and detailed profile analysis results totally corroborate each other. In the  $X[^3\text{He}]$  region from 4-6%, no trustworthy data could be obtained since the ICRF generators were struggling to couple power into the plasma, rendering the BIS/FFT analysis impossible. This effect is related to the fast-wave cut-off associated to the  $^3\text{He}$ -H mode-conversion layer, which lies close to the plasma LFS edge and hinders the penetration of the power launched by the antenna into the plasma core. When reaching  $X[^3\text{He}] > 6\%$ , the heating efficiency has fully recovered and is – apart from a weak tendency of the electron and total heating efficiency – essentially independent of the minority concentration. Whereas the behavior at low concentration is fully in agreement with what would be expected from the Fuchs et al. constructive/destructive

interference effect, the behavior at the higher concentration is at odds with it. To understand this aspect of the experimental findings it was necessary to go beyond Fuchs' model.

The cyclotron frequency being proportional to  $Z/A$ , all D-like species (sharing  $Z/A=1/2$ ) play a similar role from the ICRF heating point of view, making it difficult to discriminate between the effects they are causing individually. Although the average experimental curves could easily be identified with the corresponding confluence positions, the slope of the experimental data as a function of the  $^3\text{He}$  concentration could not be matched, while the required D-like concentrations seemed excessive. Realizing that the  $^3\text{He}$  concentration used here as a reference is the guess obtained from the real time control formula based on edge spectroscopy measurements (lacking e.g. density and temperature profile information), it seems plausible that a corrective factor should be applied to link the estimated  $^3\text{He}$  concentration with the actual one in the plasma core. A simple multiplicative correction factor of 1.6 is found via a minimization based on higher order regression. The corresponding figure with experimental and guessed concentrations is given in Fig. 5. The TOFOR neutron diagnostic allows providing a rough guess for the actual D-concentration by comparing the ratio of the beam-thermal and beam-beam neutron emission [10]. The value of  $X[\text{D}]\sim 5\text{-}7\%$  found is in good agreement with the guess provided by the minimization analysis.

## MODELLING

Kazakov [3] took the Fuchs reasoning a step further and included a second mode conversion layer and its associated cutoff. Relying on the phase integral method he found that the total mode conversion coefficient becomes  $T_1 T_2 (1 - T_1 T_2) + 4 T_2 (1 - T_2) (1 - T_1) \sin^2 \alpha / 2$  in which  $T_1$  and  $T_2$  are the transmission coefficients through the individual evanescence layers and located closer to the high and low field sides, respectively. The interference term involving the angle  $\alpha$  (the phase difference between the reflected waves) mostly depends on the distance between the cut-off/conversion layers.

Assuming the D,  $^4\text{He}$  and C concentrations that are provided by the real time control formula are trustworthy, and for the typical densities and temperatures experimentally observed, the heating efficiency for a number of toroidal mode numbers computed using the TOMCAT code [11] is shown in Fig. 6. The oscillating character of the heating efficiency as a function of the minority concentration is the consequence of the constructive and destructive interference discussed by Fuchs and by Kazakov. Minority heating is significant only at low concentration while electron heating dominates the overall absorption. Depending on the antenna phasing chosen the cumulative effect of the various toroidal modes is different. Adding several modes tends to smooth out the oscillations at the modest concentrations. Since the heating efficiency of *all* the toroidal modes degrades when approaching  $X[^3\text{He}]=4\%$ , one expects a marked decrease in the overall heating efficiency when approaching that concentration, independent of which phasing is adopted. At high  $X[^3\text{He}]$  the heating efficiency is markedly less dependent on the actual value of the concentration than it was at the lower concentrations. In between these 2 distinct regions there is a gap: just like the coupling is poor in that  $X[^3\text{He}]$  range in the experiment, the wave model

suffers. It does because a cutoff/confluence layer lies close to the antenna, preventing the wave power to reach the plasma.

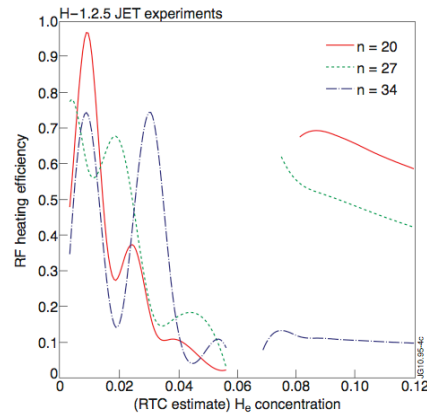


**FIGURE 6.** RF heating efficiency as a function of  $X[{}^3\text{He}]$ : sensitivity to the toroidal mode number.

## CONCLUSION/DISCUSSION

As the overall mode conversion efficiency in presence of multiple confluence layers critically depends on the confluence layers' positions, and as the latter are a function of the plasma composition, one can in principle optimize mode conversion heating by controlling the gas mixture. The extent to which this optimization is possible depends on whether the impact of non-desired particle populations (e.g. released from the wall via recycling) can be counterbalanced; in inverted scenarios this steering may be harder than in regular scenarios, both because of its sensitivity to small impurity traces in the plasma and because the FW cut-off is rapidly shifted towards the LFS for increasing minority concentration.

## ACKNOWLEDGMENTS

This work, supported by the European Communities under the contract of the Association between EURATOM and the Belgian State, was carried out within the framework of the European Fusion Development Agreement. The views and opinions expressed herein do not necessarily reflect those of the European Commission.

## REFERENCES

- [1] V. Fuchs et al 1995 *Phys. Plasmas* **2** 1637–47
- [2] D. Van Eester et al, *Plasma Phys. Control. Fusion* **51** (2009) 044007
- [3] Ye. Kazakov et al., *Plasma Phys. Control. Fusion* **52** (2010) 115006
- [4] P. Mantica et al., *Phys. Rev. Lett.* **96**, 095002 (2006)
- [5] Y. Lin, 37<sup>th</sup> EPS Conference on Plasma Physics, Dublin (2010), paper P5.164
- [6] E. Lerche et al., 37<sup>th</sup> EPS Conference on Plasma Physics, Dublin (2010), paper O4.121
- [7] E. Lerche et al., “*Experimental investigation of ICRF heating scenarios for ITER’s half-field Hydrogen phase performed in JET*”, in preparation for submission to PPCF.
- [8] M.-L. Mayoral et al., *Nucl. Fusion* **46** (2006) S-550–S-563
- [9] D. Van Eester et al., “*Enhancing the mode conversion efficiency in JET plasmas with multiple mode conversion layers*” submitted to PPCF.
- [10] C. Hellesen et al. *Rev. Sci. Instrum.* **81**, 10D337 (2010) and PhD thesis, Uppsala University, 2010
- [11] D. Van Eester et al., *Plasma Phys. Control. Fusion* **40** (1998) 1949–1975.